

An approach to coupling the gas flow dynamics and thermodynamics of hydrogen solubility in L485ME steel grade for estimation of fracture toughness

MACIEJ WITEK*
FERDINAND UILHOORN

Warsaw University of Technology, Department of Heating and Gas Systems, Nowowiejska 20, 00-653 Warsaw, Poland

Abstract The paper presents the problem of coupling the gas flow dynamics in pipelines with the thermodynamics of hydrogen solubility in steel for the estimation of the fracture toughness. In particular, the influence of hydrogen blended natural gas transmission on hydrogen solubility and, consequently, on fracture toughness is investigated with a focus on the L485ME low-alloy steel grade. Hydraulic simulations are conducted to obtain the pressure and temperature conditions in the pipeline. The hydrogen content is calculated from Sievert's law and, as a consequence, the fracture toughness of the base metal and heat-affected zone is estimated. Experimental data is used to define hydrogen-assisted crack size propagation in steel as well as to a plane strain fracture toughness. The simulations are conducted for a real natural gas transmission system and compared against the threshold stress intensity factor. The results showed that the computed fracture toughness for the heat-affected zone significantly decreases for all natural gas and hydrogen blends. The applied methodology allows for identification of the hydrogen-induced embrittlement susceptibility of pipelines constructed from thermomechanically rolled tubes worldwide most commonly used for gas transmission networks in the last few decades.

Keywords: Gas flow dynamics; Hydrogen embrittlement; Fracture toughness; Hydrogen solubility; L485ME steel grade

*Corresponding Author. Email: maciej.witek@pw.edu.pl

1 Introduction

1.1 Hydrogen induced steel embrittlement

Hydrogen-induced cracking (HIC) [1] occurs as a consequence of hydrogen (H) in atomic form diffusing through the steel surface and accumulating in the interfaces between inclusions and the steel matrix. At temperatures up to 320°C, H atoms combine with each other at the interfaces to form H₂ in a gaseous phase and increase the pressure inside the microvoids of the material microstructure. The charging of pressurized hydrogen in such places leads to disbanding of interfaces between inclusions and the steel matrix, and to forming microcracks at either one or both sides of the inclusion tips in an HIC mechanism. Another process of steel degradation associated with H diffusion into the pipe wall is hydrogen environmental assisted cracking (HEC) [1]. In this case, hydrogen atoms are absorbed and adsorbed in the crack tip region and diffuse in the fracture zone which is in front of the crack tip where the stress is highest under local loads and internal pressure [2]. Additionally, H atoms from surrounding regions also diffuses to the fracture zone through the crystal lattice. The crack propagation is caused by HEC of steel below yield strength and results in a subcritical crack growth. During the dynamic hydrogen charging, a strong interaction should exist between hydrogen diffusion and local stress in front of the crack in the notched specimens. The hydrostatic stress is formed at a distance ahead of the crack tip assists hydrogen diffusion [3].

Many hydrogen embrittlement (HE) concepts of steel degradation are presented in literature; however, commonly accepted and mostly used theories are hydrogen enhanced decohesion embrittlement (HEDE) and hydrogen enhanced localized plasticity (HELP). The concept of HEDE [4] suggests degradation due to localized reduction in cohesive strength of the iron lattice, hence the separation of cleavage planes or grain boundaries under a lower stress occurs. The embrittlement is attributed to the weakening of inter-atomic bonds, resulting in separation of atoms. The HELP mechanisms [5] assume that atomic hydrogen accelerate the dislocation mobility through an elastic shielding effect that causes a local reduction in shear stress. H transportation by dislocation motion could lead to localized high concentrations in front of crack tip. Moreover, local high strains, due to hydrogen clusters around dislocations, might disrupt interfaces and structures. The stresses at these locations increase the risk of failure. When a sufficient hydrogen concentration occurs, the local deformation process leads to brittle fracture of steel.

In study [6], the effect of a low partial hydrogen in a mixture with natural gas (NG) on the tensile, notched tensile properties, and fracture toughness of X70 pipeline steel is investigated. It is confirmed that a mixture of 10 MPa gas and 1% H₂ causes a remarkable reduction in the fracture toughness in respect of crack tip opening displacement (CTOD). As per American Petroleum Institute (API) the susceptibility of API X70 weld joints to hydrogen gas is investigated in [7], using slow strain rate tensile tests. The higher susceptibility of the weld and cross-weld specimens was primarily attributed to synergic effects between the microstructural characteristics, stress localization, and microhardness distribution, particularly, microhardness is crucial for nucleation of microcracks and a hydrogen diffusion rate induced in stress and strain localizations. Paper [8] deals with hydrogen HE susceptibility of a weld heat affected zone under thermally simulated conditions of X70 pipe steel in high pressure hydrogen gas at 20°C. Fracture mechanics Single Edge Notched Tension tests at various hydrogen pressures (0.1, 0.6, 10 and 40 MPa H₂) have been carried out. The results show that hydrogen causes a strong decrease in the

fracture toughness with increasing hydrogen pressure. The critical hydrogen pressure for the onset of HE was observed to fall between 0.1 MPa and 0.6 MPa. These results were supported by scanning electron microscope (SEM) investigations of the fracture surfaces which showed a clear shift in the fracture mode at 0.6 MPa H₂. The sample surface preparation before loading in the autoclave was found to have a significant impact on hydrogen uptake of the steel. The lowest hydrogen uptake in study [9] was found for the induction bend compared to the base material X70M. Against expectations, the hydrogen uptake decreases with increasing exposure time the induction bend as well as L485ME helical welded pipe (SAWH – helically submerged arc welded). For line tube material, similar hydrogen levels were found for different microstructures for normalized and thermomechanically rolled pipes. For tube base material, the different hydrogen uptake may be attributed to a higher alloy content in the pipe. In order to obtain a combination of mechanical properties required for certain steel grades, a precise selection of alloying elements is necessary. However, some alloying components have an adverse influence on the embrittlement susceptibility of pipeline steels through introducing microstructural features that ultimately affect both diffusion and solubility of hydrogen. This effect is highly dependent on the manufacturing process as well as on heat treatment resulting in different microstructures of the base material [10]. The service degradation of Kh70 steel grade is studied in [11] and showed a considerable drop of Charpy energy, decrease in fracture toughness and reduced resistance to fatigue crack growth. The performed analysis of the resistance of the pipeline steels to the corrosion fatigue crack nucleation and growth and the respective recommendations are provided concerning the avoidance of the stress corrosion failure of gas transmission system.

1.2 Fracture toughness of low-alloy steel

Fracture toughness is a measure of the material ability to contain defect such as a crack; the higher value, the more resistant is the material to the crack extension. Fracture toughness values are typically presented in the literature in terms of plane strain fracture toughness (K_{IC}) for linear elastic materials, elastic-plastic fracture toughness is usually characterized by of J-integral (J_{IC}), crack growth resistance curves such as the slope of the fracture resistance curve related to the tearing capability of the material. The elastic-plastic method overall involves generation of J-R (J Resistance) curve for the material which is a plot of the steel resistance to crack extension using the J-integral as a function of stable crack extension. Elastoplastic fracture mechanics is applicable for ductile materials such as low-alloy carbon steel. If non-linear local steel deformation is confirmed to a small region around the crack tip, a plastic zone is small in comparison to the defect dimensions, linear plastic fracture mechanics can be applied.

However, for small scale yielding applicable in a concept of hydrogen embrittlement of steels, a target stress intensity factor is usually called fracture toughness. Linear fracture mechanics applied to an initiated crack as well as hydrogen-assisted propagation under cyclic or quasi-static loading may be used in a structural assessment of the pipeline life [12]. Wang [13] showed that the fracture toughness of L485ME steel grade declines with the rise in H₂ concentration achieved under steady-state charging conditions for specimens with the hydrogen. According to publication [3], a decrease in fracture toughness of X70 steel grade depends on several factors such as: (i) hydrogen charging condition and electrochemical charging current, (ii) hydrogen content and distribution in the materials, and (iii) dominant hydrogen embrittlement mechanisms, HELP or HEDE.

The observed fracture toughness degradation is influenced by multiple factors such as: (i) hydrogen concentration, (ii) pH value of the environment, (iii) corrosion rate of low carbon steel and (iv) degree of an activity and predominance of particular HE mechanisms, HELP or HEDE. It is worth mentioning that the decline in fracture toughness and a crack propagation phenomenon was detected and confirmed in different grades of steels, due to multiple active HE mechanisms (HELP + HEDE) [3]. This decrease is independent of activity and predominance of a particular HE mechanism, i.e., it was confirmed both in the case of dominance of HELP and HEDE mechanisms and also due to their synergistic action [3]. Despite numerous studies on possible hydrogen embrittlement mechanisms in steels published and summarized in comprehensive review such as [15], there is still no consensus among researchers on all HE mechanisms and their interactions.

The novelty of this work is the proposed methodology of estimation of the pipeline operating conditions using a dynamic flow model and the material fracture toughness determination. The latter parameter is evaluated against threshold values obtained from experimental data. In particular, the following issues are addressed in the present study:

- calculation of the hydrogen content in the tube wall base material and the heat affected zone using Sievert's law together with a nonisothermal transient gas flow model;
- calculations and experiments are used to compare a fracture toughness parameter, namely, a computed conditional stress intensity factor, with the threshold stress intensity factor for plane strain environmentally-assisted cracking;
- hydrogen-assisted crack size propagation in steel specimens is compared to the subcritical crack growth obtained from constant displacement method measurements and macroscopic/microscopic evaluation;
- estimation of a decrease in fracture toughness as a function of dynamic hydrogen charging in the pipe wall of L485ME steel grade.

2 Standardized fracture control qualification test of pipeline steel

A fracture toughness criterion or other method shall be specified to control fracture propagation when a pipeline suitable for transportation of C_xH_y/H_2 blends is designed to operate at a hoop stress over 40% of the specified minimum yield strength. When a fracture toughness criterion is applied, control shall be achieved by ensuring that the tube material presents adequate ductility. The tube material tensile requirements shall be specified on the purchasing specification and shall comply with the chemical and tensile requirements of EN-ISO 3183:2019 [16] and API 5L [17].

In this paper, Option B according to ASME B31.12 [18] was applied with the following requirements. The pipe and weld material shall be qualified for adequate resistance to fracture in H_2 gas at or above the design pressure and at ambient temperature using the applicable rules provided in Article KD-10 of ASME BPV Code Section VIII, Division 3 [19]. The purpose of this test is to qualify the material of the structure by testing three heats of the steels. The threshold stress intensity factor values (K_{IH}) shall be obtained from the thickest section from each heat of the material and a type of the

applied heat treatment. The test specimens shall be in the final heat-treated condition to be used in pipe manufacturing. A set of three specimens shall be tested from each of the following locations: base metal (BM), weld metal (WM) on the tube body, and heat-affected zone (HAZ) of joints, welded with the same qualified welding procedure specification as intended for the piping manufacturing. A change in the welding procedure requires retesting of welded joints in the scope of WM and HAZ. The test specimens shall be in the transverse longitudinal (TL) axis of forcing direction. If TL specimens cannot be obtained from the weld metal and the heat affected zone, then longitudinal transverse (LT) oriented specimens may be used. The values of K_{IH} shall be obtained with the use of the test method described in KD-1040 of ASME BPV Code Section VIII, Division 3 [19]. The lowest measured value of K_{IH} shall be used in the pipeline design analysis.

The values obtained as described above may be used for other tubes manufactured from the same material specification (steel grade) or similar material specification with the same nominal chemical composition, and the same heat treatment condition, providing its tensile and yield strengths do not exceed the values of the material used in the qualification tests by more than 5%. The welded joints shall meet the requirements of the welding procedure specification used for qualifying the construction material. Calculation of the maximum applied stress intensity factor (K_{IA}) required at design pressure is for the elliptical surface crack. The critical crack size is developed by applicable fatigue loading. Fatigue design rules specified in Article KD-1010 shall be used, or depth equals $t/4$, length equals $1.5t$, where t is the pipe wall thickness. Determination of threshold stress intensity factor K_{IH} in H_2 gaseous atmosphere by applying the test method, as specified in KD-1040.

Additional requirement for the pipe material are as follows:

- phosphorus (P) content of the tube shall not exceed 0.015% by weight;
- sulphur (S) – the maximum content for welded as well as seamless pipes is 0.010% by weight;
- the tube material shall be manufactured with a practical control of inclusions;
- minimum specified yield strength shall not exceed 555 MPa, maximum ultimate tensile strength of the weld metal shall not exceed 760 MPa and tube shall meet all applicable requirements of EN-ISO 3183:2019 [16] and API PSL2 [17];
- brittle and ductile specified in ASME B31.12 [18] shall be met.

2.1 Hydrogen embrittlement experiments for L485ME steel grade

The mechanical properties, such as yield and tensile strength, hardness as well as a chemical composition of L485ME steel grade of 10 selected tubes produced by Corinth Pipe-works S.A. [20], are presented in Appendix A. In the case of pipes used for experiments in the present study both hardness criterion set as less than 235 HV10 as well as percentage of selected micro additives determined as $S \leq 0.010\%$, $P \leq 0.0156\%$ are met. The steps applied for experimental evaluation of fracture toughness and crack size extension are defined according to KD-1041 [19]:

- The modified bolt-load specimen configuration as presented in Fig. 1 was utilized in accordance with ASTM E1681-03 international standard [21]. Base metal, weld metal centre line and HAZ testing locations were used as samples. Thirty-six L485

ME steel grade specimens from BM (12 specimens), WM (12), HAZ (12), were prepared from 14.2 mm SAWH pipe for fatigue pre-cracking testing, at ambient temperature, in general compliance with ASTM E1681-03 code.

- A machined notch was further extended through fatigue pre-cracking in ambient temperature conditions. Fatigue pre-cracking testing was performed using Instron Fatigue Propagation Program – Version 8.1 Build 4 following the test control parameters: range – 33 MPam^{0.5}, stress ratio – 0.100, points/cycle – 200, waveform sine frequency – 25 Hz.
- Specimen bolt-loading (crack opening) was performed in an inert atmosphere (pure N₂) in which oxygen and moisture were stored, and continuously monitored, below 5 and 50 ppm respectively, as required by the ASME code [18].
- According to the requirements of ASTM E1681 standard [21], the original pre-crack size (a_o) was measured after fracture at five locations, as presented in Fig. 1:
 - at the centre of the crack front ($a_o(1/2)$),
 - halfway the centre of the crack front ($a_o(1/4)$ and $a_o(3/4)$),
 - at the ends of the crack front on each side surface ($a_o(L)$ and $a_o(R)$).
- The applied displacement (V_m) was measured with the use of a CMOD-type electronic extensometer. Based on ASTM E1681-03 [21] equation in §9.1.3, the applied displacement was calculated for all specimens in order to exceed the minimum required value of applied stress intensity factor $K_{IA} = 110$ MPam^{0.5}, with a typical target of $K_{IA} = 125$ MPam^{0.5}. According to the provisions of standard ASME BPVC Sec. VIII, Division 3, KD-1041 [19], minimum stress intensity factor $K_{IH,min}$ is equal to 50% of K_{IA} , if the test was applied using the constant displacement method.
- Having completed the loading of specimens, they were placed in the autoclave which was closed tightly.
- Next, before being charged with high purity H₂ (grade 6.0), the autoclave was filled with high purity N₂ (grade 6.0) and the pressure was elevated to test value. The working pressure for the experiment was set at a minimum of 8 MPa for a duration of 1000 h.

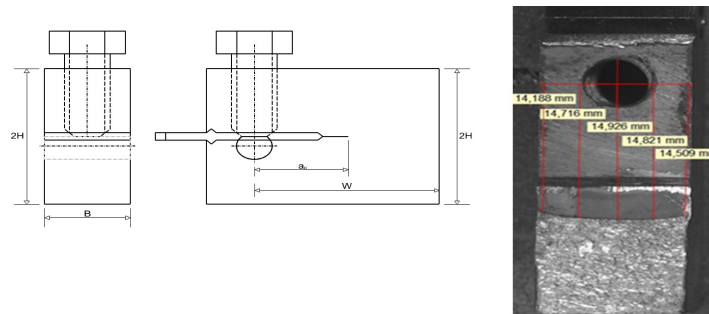


Figure 1: Bolt-load specimen for constant displacement and locations of crack size measurements [20].

- In order to highlight any potential crack propagation, the specimens were heat tinted in the furnace for 1 h and subsequently broken in liquid nitrogen. According to the requirements of ASTM E1681-03 code [21], evaluation of a crack growth caused by hydrogen was conducted perpendicular to the pre-crack at 25% B , 50% B and 75% B locations, where B is the specimen thickness. The results of a target and measured crack size (a_o), applied displacement (V_m), values of target and applied stress intensity factor (K_{IA}) as well as minimum stress intensity factor ($K_{IH,min}$) are presented for representative specimens in Appendix B [20]. According to the evaluation of the specimens, no subcritical crack growth more than 0.25 mm average on three locations was identified for a minimum of three specimens tested per a position. The table in Appendix B presents in details the measurements of the crack size and fracture toughness values for L485ME steel grade, for thickness of specimens – 12.5 mm, width – 25 mm, and height – 12.1 mm. Transverse longitudinal orientated specimens were taken from BM (12 specimens), WM (12), HAZ (12), from SAWH pipes with the wall thickness of 14.2 mm.
- Post-test macroscopic evaluation of specimens as well as evaluation with Scanning Electron Microscope are presented in the next subchapter.

2.2 Macroscopic and microscopic examination of the specimens

All the prepared samples were analysed macroscopically and using the electron microscopy. Macroscopic examination of the sample was performed with the use of Nikon SMZ 1500 stereo-microscope. Observations with a higher magnification microscope were performed with JEOL IT-800 HL SEM under 20 kV accelerating voltage, coupled with EDAX Octane Elect Plus system with the usage of TEAM software. The results of selected macroscopic examinations are presented in Figs. 2(a)–(c), whereas representative electron micrographs are shown in Figs. 3(a)–(c). Similar results were observed in the remaining samples, as listed in Appendix B. Therefore, no HIC was detected in 36 examined samples.

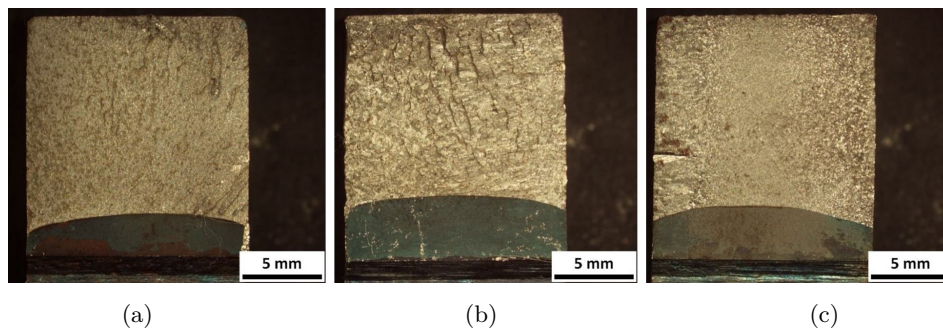


Figure 2: Macrographs of fracture surfaces of (a) S203A BM1, (b) S203A W4 and (c) S203A HAZ4 [20].

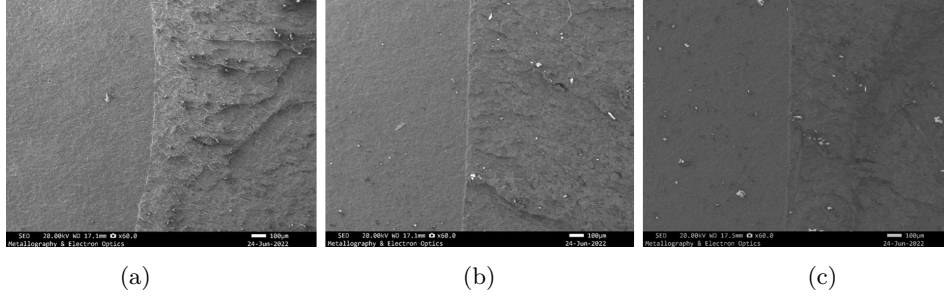


Figure 3: Electron micrographs (SEM) showing the interface between the fatigue and the crack initiation zone of the fracture surface at (a) 25%, (b) 50%, and (c) 75% of the S203A-BM1 specimen width [20].

3 Coupling of flow dynamics, hydrogen solubility and fracture toughness

In this section, the governing equations of the compressible flow model, thermodynamics of hydrogen solubility at equilibrium and empirical correlations for the fracture toughness are presented. The flow model is used to compute the pressure and temperature conditions in the pipeline. The results are used to calculate the hydrogen content in the tube wall using Sievert's law. The fracture toughness can be estimated from the hydrogen content. It is assumed that thermodynamic equilibrium exists between the steel and hydrogen in the gas mixture. This modeling approach allows for identification of the time and location where HE might cause a detrimental failure.

3.1 Gas flow model

The flow model constitutes a non-homogeneous hyperbolic system of partial differential equations derived from the conservation principles of mass, momentum, and energy. The governing equations can be written as [22, 23]:

$$\frac{\partial \mathbf{U}}{\partial t} + \mathbf{F}(\mathbf{U}) \frac{\partial \mathbf{U}}{\partial x} + \mathbf{S}(\mathbf{U}) = 0, \quad \forall x \in \mathbb{R}, \quad t \in \mathbb{R}^+, \quad (1)$$

with

$$\mathbf{F}(\mathbf{U}) = \begin{bmatrix} -\frac{\dot{m}(a_s^2 \alpha_2 - RTz)}{A p} & \frac{a_s^2}{A} & \frac{a_s^2 \dot{m} \alpha_1}{AT} \\ A - \frac{a_s^2 \alpha_2^2 c_p \dot{m}^2 - Ra_s^2 \alpha_1^2 \alpha_2 \dot{m}^2 z}{Ac_p p^2} & \frac{\dot{m}(\alpha_2 c_p a_s^2 - Rz a_s^2 \alpha_1^2 + RT c_p z)}{Ac_p p} & \frac{a_s^2 \alpha_1 \dot{m}^2 (\alpha_2 c_p - R \alpha_1^2 z)}{AT c_p p} \\ -\frac{RT a_s^2 \alpha_1 \alpha_2 \dot{m} z}{Ac_p p^2} & \frac{RT a_s^2 \alpha_1 z}{Ac_p p} & \frac{R \dot{m} z (a_s^2 \alpha_1^2 + T c_p)}{Ac_p p} \end{bmatrix}, \quad (2)$$

and

$$\mathbf{S}(\mathbf{U}) = \begin{bmatrix} -\frac{a_s^2 \alpha_1 (\Omega A p + RT \dot{m} f_r z)}{A^2 T c_p p} \\ f_r + \frac{p A g}{z T R} \sin \theta \\ -\frac{a_s^2 \alpha_2 (\Omega A p + RT \dot{m} f_r z)}{A^2 c_p p^2} \end{bmatrix}. \quad (3)$$

The parameters α_1 and α_2 are defined as follows:

$$\alpha_1 = 1 + \frac{T}{z} \left(\frac{\partial z}{\partial T} \right)_p, \quad \alpha_2 = 1 - \frac{p}{z} \left(\frac{\partial z}{\partial p} \right)_T. \quad (4)$$

The state vector is defined as $\mathbf{U} = [p \quad \dot{m} \quad T]$ and the following initial and boundary conditions are as follows:

$$p(x, 0) = p_0(x), \quad T(x, 0) = T_0(x), \quad (5)$$

$$p(0, t) = p_0, \quad \dot{m}(L, t) = \phi(t), \quad T(0, t) = T_0, \quad (6)$$

where $\phi(t)$ is the outflow demand. Other variables and parameters are pressure p , mass flow rate \dot{m} , temperature T , cross-sectional area A , frictional force w , friction factor f_r , gravitational acceleration g , angle of inclination θ , rate of heat transfer Ω , specific gas constant R , compressibility factor z , and specific heat at constant pressure c_p . The isentropic wave speed a_s is calculated as follows:

$$\left(\frac{\partial p}{\partial \rho} \right)_s = \left[\frac{\rho}{p} \left(1 - \frac{p}{z} \left(\frac{\partial z}{\partial p} \right)_T - \frac{p}{\rho c_p T} \left(1 + \frac{T}{z} \left(\frac{\partial z}{\partial T} \right)_p \right)^2 \right) \right]^{-1}. \quad (7)$$

The frictional force w per unit length is defined as

$$w = \frac{1}{8} f_r \rho v |v| \pi d_i, \quad (8)$$

with velocity v and internal diameter d_i . The friction factor is calculated from [24]:

$$f_r = -0.8685 \ln \left(\frac{1.964 \ln(\text{Re}) - 3.8215}{\text{Re}} + \frac{\varepsilon}{3.71 d_i} \right)^{-2}, \quad (9)$$

where ε denotes the roughness and Re is the Reynolds number.

The steady heat transfer between the fluid and soil per unit length and time is defined as:

$$\Omega = -\pi d U (T - T_s), \quad (10)$$

where U is the total heat transfer coefficient and consists of the heat transfer between the gas and the inner wall, heat transfer through the pipe wall, and heat transfer between the outer wall and soil with temperature T_s . For a pipeline with three different layers, it can be defined as follows:

$$U = \left(\frac{1}{h_i} + r_1 \frac{\ln(r_2/r_1)}{k_1} + r_1 \frac{\ln(r_3/r_2)}{k_2} + r_1 \frac{\ln(r_4/r_3)}{k_3} + \frac{r_1}{r_3 h_o} \right)^{-1}, \quad (11)$$

where k and r refer to the thermal conductivity and a radius of the wall layer, respectively. The heat transfer from the gas to the wall is given by

$$h_i = \text{Nu} \frac{k_{\text{gas}}}{d_i}, \quad (12)$$

where k_{gas} is the thermal conductivity of the fluid. The Nusselt number is obtained from the Dittus-Boelter correlation [25]:

$$\text{Nu} = 0.023 \left(\frac{4\dot{m}}{\pi d \mu} \right)^{4/5} \left(\frac{c_p \mu}{k_{\text{gas}}} \right)^{0.3}. \quad (13)$$

The heat transfer coefficient between the outer wall and soil is defined as:

$$h_o = \frac{k_{\text{soil}}}{\left(\frac{d_o}{2} \right) \cosh^{-1} \left(\frac{2Z}{d_o} \right)}, \quad (14)$$

where k_{soil} is the thermal conductivity of the soil, and Z is the distance between the top of the soil and the center of the pipe. The equation of state (EOS) GERG-2008 [26], which is explicit in the Helmholtz free energy as a function of density, temperature, and composition, is used to calculate the thermodynamic properties.

For the numerical approximation of Eq. (1), a semidiscretization approach is used, where the flow model is converted into a set of ordinary differential equations (ODEs) by the discretization of the spatial derivatives. The system of ODEs can be written as:

$$\frac{d\mathbf{u}(t)}{dt} = -\mathbf{F}(\mathbf{u})\mathbf{T}\mathbf{u}(t) - \mathbf{S}(\mathbf{u}(t)) = f(\mathbf{u}(t)), \quad (15)$$

where $\mathbf{T} = \sum_{j=1}^n \mathbf{I}_j \otimes \mathbf{T}^{(j)}$, and $n = 3$ and $\mathbf{T}^{(j)} = \mathbf{T}^{(1)} \forall j$, where the coefficients can be

found in [27] and refer to a classical five-point, fourth-order finite-difference approximation. For the integration of $f(\mathbf{u}(t))$, the TR-BDF2 scheme [28] is used. The implementation of this scheme can be found in [29, 30]. The sparsity of the ODEs is exploited to reduce the computation time.

3.2 Hydrogen solubility computations

In thermodynamic equilibrium, the chemical potential of hydrogen in gaseous phase $\mu_{\text{H}_2}^{\text{gas}}$ and hydrogen dissolved in steel $\mu_{\text{H}}^{\text{M}}$ should be equal, i.e., $1/2\mu_{\text{H}_2}^{\text{gas}} = \mu_{\text{H}}^{\text{M}}$ [31]. This condition leads to Sievert's law and is frequently used to describe the hydrogen solubility of metals. The details concerning its derivation can be found, for example, in [32]. Drexler *et al.* [33] extended Sievert's law to low temperatures and high gas pressures, considering microstructural trapping sites, fugacity, and multiaxial stress states in the following manner:

$$c_{\text{H}} = k_0 \sqrt{f} \exp \left(-\frac{\Delta H_s - \sigma_H V_H}{RT} \right), \quad (16)$$

where k_0 is the solubility coefficient, f is the fugacity of hydrogen, ΔH_s is the change of the solution enthalpy, σ_H is the hydrostatic stress, and V_H is the partial molar volume of hydrogen in solid solution. The solubility coefficient is defined as [34]:

$$k_0 \cong k'_0 \left(\frac{N_T}{N_L} + \frac{N_T}{N_L K_T} + 1 \right), \quad (17)$$

where k'_0 is a constant pre-factor, and $K_T = \exp(-E_b/RT)$ where N_L and N_T are the densities of the lattice and trap sites, respectively, and E_b is the trap binding energy. The hydrostatic stress for thin-wall pipelines ($d/t_w > 20$) is approximated by

$$\sigma_H = \frac{pr_i}{2t_w}, \quad (18)$$

with internal radius r_i and wall thickness t_w . It is assumed that the material is linear-elastic, isotropic, and homogeneous, and the stress distributions throughout the wall do not vary. To calculate the hydrogen solubility from Eq. (16), the flow model (1) is used to obtain the gas pressure and temperature. The fugacity of hydrogen in the natural gas mixture is calculated from GERG-2008.

3.3 Fracture toughness calculations

Based on experiments, Wang [13] introduced a correlation for the conditional fracture toughness K_{IQ} according to ASTM E-399-22 [35] as a function of hydrogen concentration under hydrogen pre-charging $K_{IQ,p}$ and dynamic charging $K_{IQ,d}$ at slow strain rate tension for line tube steel API X70. The corresponding correlations are:

$$K_{IQ,p} = 91.29 - 2.15c_H \quad (19)$$

and

$$K_{IQ,d} = 58.31 - 19.84 \log c_H \quad (20)$$

respectively. These correlations are used to calculate the fracture toughness of the steel pipeline. However, it is required to perform this estimation carefully for two reasons. Firstly, the chemical composition of the steel, on which the correlations are based, is slightly different (see Table 2). Secondly, it is unknown how well electrochemical hydrogen charging reflects the process of hydrogen diffusion in pipelines under transient flow conditions. Nevertheless, an attempt is made to indicate the fracture toughness for these two scenarios.

4 A real case study

For the case study, the Yamal pipeline section on Polish territory between compressor stations CS-1 and CS-2 is considered (see Fig. 4). The pipeline length is 177 km and is made of steel X70M with an internal diameter of 1379.6 mm and roughness of 1.96 μm . The thickness of the pipe wall is 19.22 mm and its thermal conductivity is 45.3 $\text{W m}^{-1}\text{K}^{-1}$. In Section 2, L485ME steel grade was investigated. The relationship between the case study and Section 2 is that the steel grades can be considered as similar. The Yamal gas transmission pipeline is manufactured from X70M steel grade, according to the European standards from the 1990s. The chemical composition of X70M does not significantly differ from L485ME steel grade used in the experiments, according to EN-ISO 3183 [16] established in 2019. Nevertheless, as pointed out in Section 3.3, care should be taken because of the slight difference in chemical composition.

The soil temperature is 285.15 K and its thermal conductivity is 2.0 $\text{W m}^{-1}\text{K}^{-1}$. The pipeline depth is 1.5 m. The boundary condition $\dot{m}(Lt) = \phi(t)$ is based on averaged daily values measured in 2020 (see Fig. 5) and the discharge pressure and temperature are set at

$p(0, t) = 8.4$ MPa and $T(0, t) = 290.15$ K, respectively. The service days of the compressors are excluded, and as a result, the simulation period is 351 days. To avoid instability of the compressors, the surge pressure at CS-2 should not drop below 4.9 MPa. The natural gas has the following composition in mol %: 96.803 CH₄, 1.773 C₂H₆, 0.395 C₃H₈, 0.063 *i*-C₄H₁₀, 0.057 *n*-C₄H₁₀, 0.010 *i*-C₅H₁₂, 0.007 *n*-C₅H₁₂, 0.009 C₆, 0.115 CO₂, and 0.768 N₂. At node 1, the hydrogen is blended with the natural gas with different volume percentages, namely, 10%, 25%, and 50%.

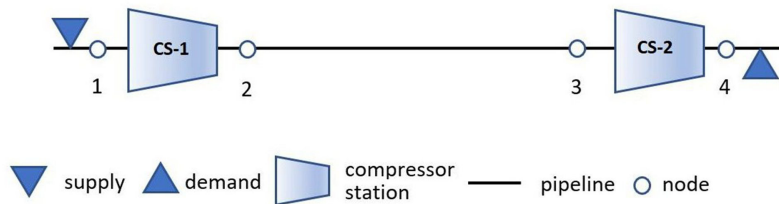


Figure 4: Schematic of the high-pressure pipeline.

The simulations are conducted for BM and HAZ with the parameters given in Table 1. The number of trapping sites per unit volume N_L and binding energy E_b are based on work presented in [14, 36]. These values are estimated from the effective diffusion coefficient for steel with a composition as shown in Table 2. The base metal consisted mainly of a fine-grained ferritic structure, while the HAZ material consisted of a mixture of ferrite and martensite/martensite-austenite due to microstructural alternations taking place during welding.

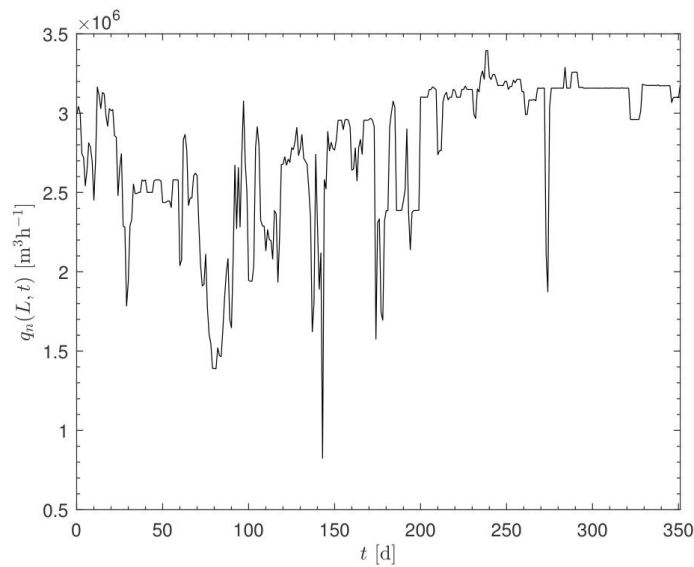


Figure 5: Flow rate boundary condition $\phi(t)$ at $x = L$.

Table 1: Parameters used for estimating the hydrogen content [14, 33, 36].

Parameters	Values	Units
Binding energy for BM, $E_{b, \text{BM}}$	36	kJ mol^{-1}
Binding energy for HAZ, $E_{b, \text{HAZ}}$	41	kJ mol^{-1}
Trap density, N_T	$2.3 \cdot 10^{19}$	sites cm^{-3}
Constant pre-factor,	33	$\text{wppm bar}^{-0.5}$
Partial molar volume of H_2 , V_h	$2 \cdot 10^3$	$\text{mm}^3 \text{mol}^{-1}$
Solution enthalpy, ΔH_s	27	kJ mol^{-1}
Number of lattice sites, N_L	5.2×10^{23}	sites cm^{-3}

Table 2: Chemical composition of X70 steels [13, 14].

	C	Mn	Si	P	S	Cu	Ni	Al	Nb	V	Cr	Mo	Ti	N	Fe
Olden <i>et al.</i> [14]															
BM	0.09	1.71	0.3	0.012	0.001	0.04	0.05	0.05	0.05	0.01	0.07	0.02	0.02	0.005	
HAZ	0.047	1.74	0.1	0.01	0.007	0.22	0.25	0.027	0.027	0.001	0.047	0.042	0.01	0.0025	
Wang [13]															
–	0.041	1.76	0.281	0.016	0.006	0.193	–	–	0.067	–	–	0.194	0.023	–	balance

The variations in pressure and temperature at node 3 are shown in Fig. 6. The difference in pressure drop between the mixtures is caused by the lower viscous resistance. The temperature change is caused by the radial convective and conductive heat transfer, accumulation in the soil, and the Joule-Thomson effect [37]. In this work, the simulations are conducted with the same volumetric flow. Blending hydrogen into natural gas decreases the energy density per m^3 . To compensate for the latter effect, the gas flow rate should be increased, which will change the flow conditions in the pipeline, and as a result, the hydrogen content in the steel.

The estimated hydrogen content in the steel pipeline for different amounts of hydrogen in natural gas is shown in Fig. 7. The minimum and maximum values are summarized in Table 3 together with the corresponding pressure and temperature. These values are the solutions at each discretization node of the numerical flow model. Compared to BM, the highest hydrogen concentrations are observed for HAZ, with maximum values of 1.91 (10% vol. H_2), 2.95 (25% vol. H_2), and 4.07 wppm (50% vol. H_2). The structure of HAZ is composed of bainite and martensite, while BM is mainly composed of ferrite. During the martensitic transformation, the residual stress and dislocations increase, including the number of trap sites, and as a result, the hydrogen concentration becomes higher. The corresponding maximum values for BM are 0.23, 0.36 and 0.50 wppm. The lowest values, for both BM and HAZ, are noticed at node 2 and $t = 0$, while the maximum values are observed at node 3 and $t = 143$ days.

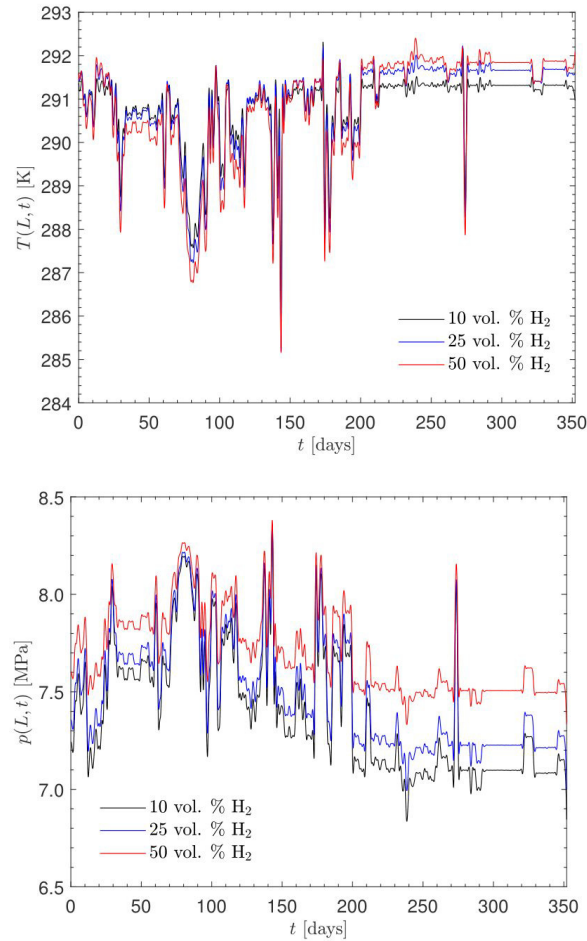


Figure 6: Pressure and temperature evolution for 10%, 25% and 50% vol. H₂ in NG.

In [36], an average effective hydrogen diffusion coefficient at room temperature of $7.60 \cdot 10^{-11} \text{ m}^2 \text{ s}^{-1}$ (BM), $4.01 \cdot 10^{-11} \text{ m}^2 \text{ s}^{-1}$ for weld metal and $1.26 \cdot 10^{-11} \text{ m}^2 \text{ s}^{-1}$ for HAZ was found. As it can be observed from the above data, base metal on the pipe body showed a higher effective diffusion coefficient compared to the weld material of L485ME steel grade as well as heat affected zone on tube. An increased alloying level of steel tends to slow down hydrogen diffusion through the tube wall.

To calculate the stress-enhanced hydrogen solubility in pressurized specimens, pipes, and pressure vessels, Drexler *et al.* [38] used the following parameters: $E_b = 30 \text{ kJ mol}^{-1}$, $N_T = 10 \cdot 10^{-7} \text{ mol mm}^{-3}$, and $N_L = 8.5 \cdot 10^{-4} \text{ mol mm}^{-3}$. These parameters are considered a rough estimation for ferritic and martensitic steels. The remaining parameters are the same as in Table 1. The results for these parameters are shown in Table 3, and show

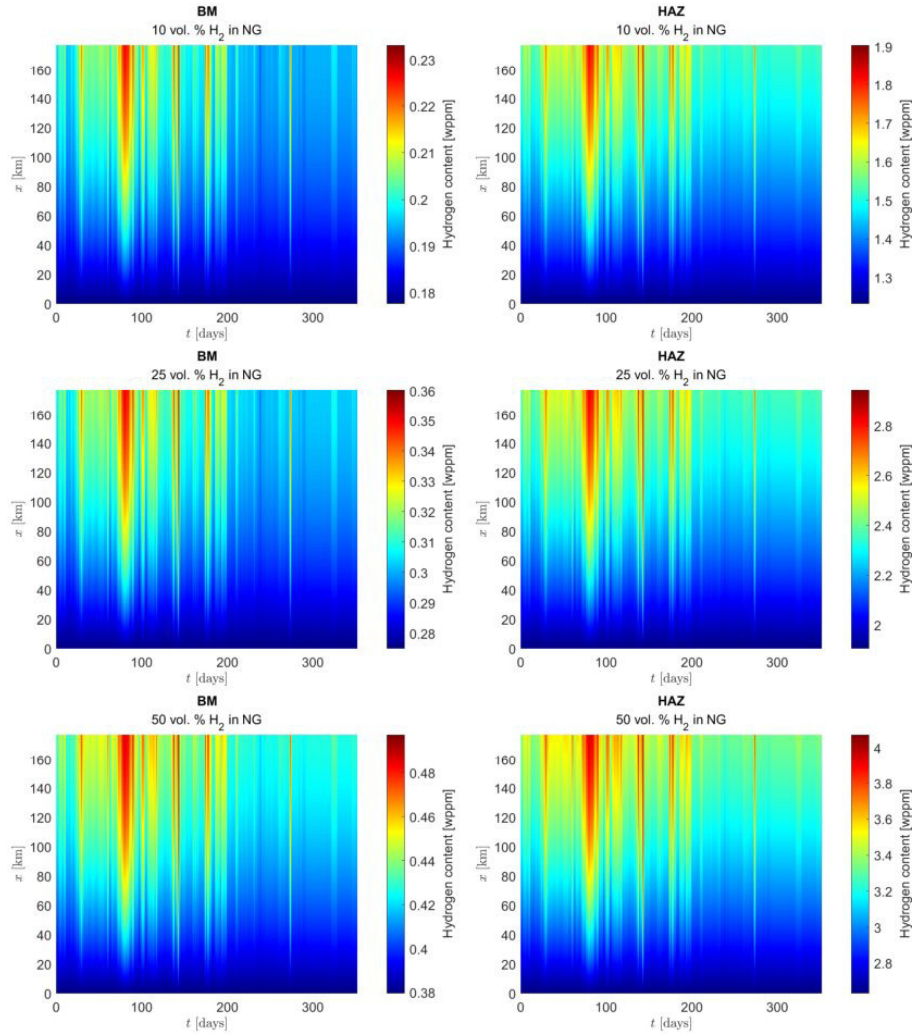


Figure 7: Hydrogen content for BM and HAZ with 10%, 25% and 50% vol. H₂ in NG.

significantly lower values for the hydrogen content. It was noticed that the binding energy has a strong influence on the calculated hydrogen content. This parameter depends on the material imperfections, the interatomic forces between hydrogen and iron at the defect sites, and the dilation of the crystal lattice nearby the crystal defects [38].

The results are depicted in Fig. 8 and summarized in Table 3. Compared to BM, the fracture toughness of HAZ significantly decreases for all C_xH_y/H_2 blends. The validity of comparison of threshold stress intensity factor K_{IH} [21] with conditional calculated values $K_{IQ,p}$ and $K_{IQ,d}$ [13] are ensured by size requirements of the specimens [21, 35] meeting criteria for plane strain conditions.

Table 3: Estimated maximum hydrogen content and minimum fracture toughness [14, 36, 38].

H ₂ (vol. %)	$c_{H,\min}$ (wppm)	p, T (MPa), (K)	$K_{IQ,p}$ (MPa m ^{0.5})	$K_{IQ,d}$ (MPa m ^{0.5})	$c_{H,\max}$ (wppm)	p, T (MPa), (K)	$K_{IQ,p}$ (MPa m ^{0.5})	$K_{IQ,d}$ (MPa m ^{0.5})
BM [14, 36]								
10	0.18		90.9	92.6	0.23	8.23, 285.8	90.8	87.2
25	0.28	8.45, 308.15	90.7	83.9	0.36	8.27, 285.7	90.5	78.6
50	0.38		90.5	77.5	0.50	8.31, 285.4	90.2	72.1
HAZ [14, 36]								
10	1.23		88.6	54.2	1.91	8.17, 285.5	87.2	45.6
25	1.91	8.45, 308.15	87.2	45.5	2.95	8.22, 285.4	85.0	36.9
50	2.63		85.6	39.1	4.07	8.23, 285.3	82.5	30.5
Ferritic and martensitic steels [38]								
10	0.04	6.84, 291.3	91.2	120.5	0.05	8.32, 286.8	91.2	117.4
25	0.07	7.00, 291.9	91.1	111.6	0.08	8.34, 286.5	91.1	108.8
50	0.10	7.33, 292.4	91.1	104.6	0.11	8.37, 286.0	91.1	102.4

Information concerning the allowable hydrogen content and fracture toughness enables to demarcate the location and time where HE might appear. Wang [13] found a critical hydrogen concentration of 1 wppm for the X70 pipeline steel, at which the fracture toughness is significantly reduced. The results in Table 3 show that the hydrogen content of HAZ exceeds this critical concentration. From the experimental results reported in Appendix B, a mean $K_{IH,\min}$ of 66.0 and 65.4 MPa m^{0.5} was found for BM and HAZ, respectively. According to KD-1041 [19], if the test was conducted using constant displacement method, $K_{IH,\min}$ is equal to 50% of the applied K_{IA} . Taking into account that K_{IA} values exceed 110 MPa m^{0.5} for all specimens, the threshold stress intensity factor K_{IH} value of 55 MPa m^{0.5} can also be qualified as a minimum for all specimens. The latter value is used to evaluate the fracture toughness of L485ME steel that is exposed to hydrogen. The second condition for the material characterization of pipelines and pressure vessels with respect to hydrogen induced cracking is that the defect growth exhibited by the experiments does not exceed 0.25 mm. Simulation results show that only the HAZ material seems to be vulnerable to HE. This would imply that the injection of 10%, 25%, and 50% vol. H₂ in the natural gas for the BM material and parameters used for ferritic and martensitic steels may not cause fracture toughness problems for L485ME steel grade. By all means, the results are valid within the assumptions and approximations considered in the case study.

The advantage of the proposed methodology is a possibility to forecast in long time operation that hydrogen environmental cracking may cause a detrimental failure at specific pipeline locations. Moreover, a positive is that the modeling approach can be applied to any low alloyed steel tubes carrying hydrogen blended natural gas. The disadvantage is

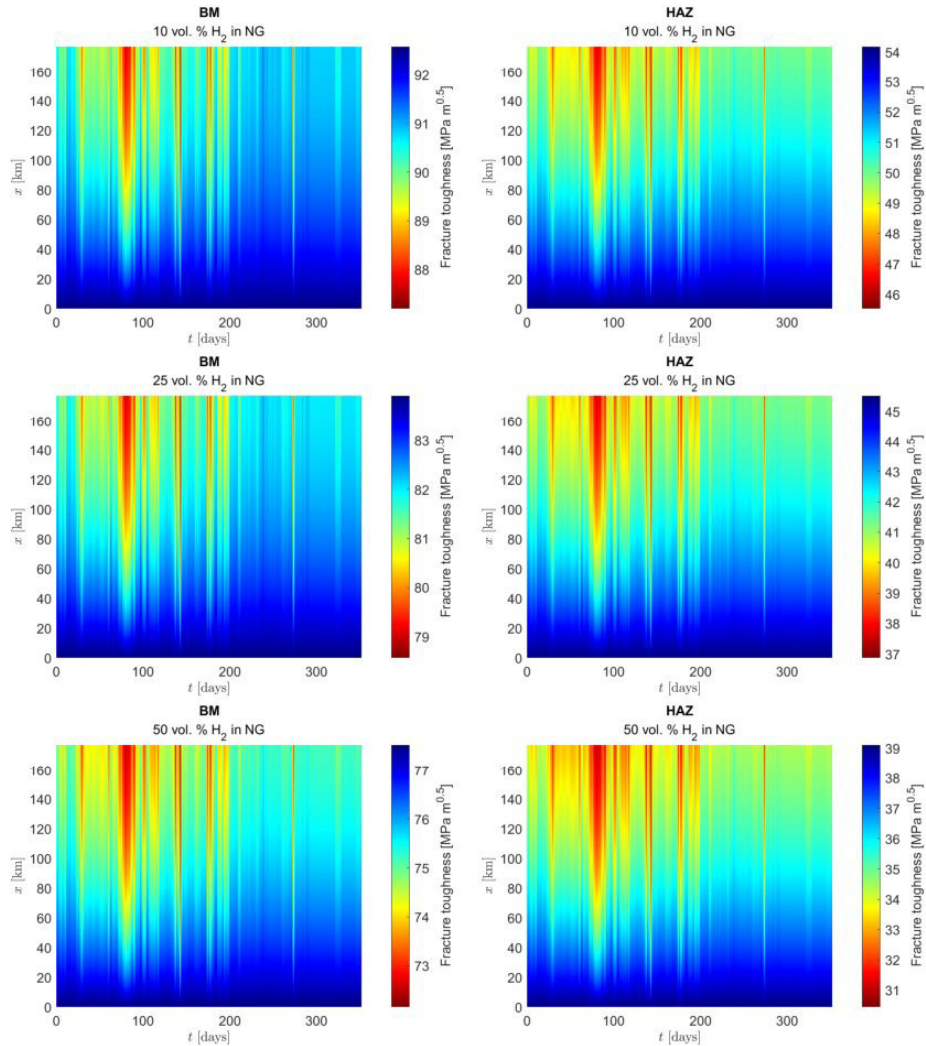


Figure 8: Fracture toughness according Eq. (20) for BM and HAZ with 10%, 25% and 50% vol. H₂ in NG.

the uncertainty in acquiring accurate data of the properties required to calculate the hydrogen content (e.g. binding energy, trap density, number of lattice sites) and as a result, the fracture toughness. This also concerns parameters used in the flow model, for example, the soil temperature and properties such as heat capacity and a thermal conductivity change over time, as it alternately wets and dries. These quantities are difficult to determine; however, they can significantly affect a transient flow in the pipeline, particularly the temperature of the gas mixture.

5 Conclusions

In this work, the hydrogen content and fracture toughness were calculated for the L485ME low-alloy steel grade that is worldwide used for the construction of gas transmission networks. A transient non-isothermal flow model was used to estimate the pressure and temperature conditions in the pipeline. From Sievert's law, the hydrogen content was calculated, and as a consequence, the fracture toughness of the base metal and heat-affected zone was obtained. The simulation results were compared against the experimental threshold stress intensity factor and showed that the computed fracture toughness for HAZ significantly decreases for all C_xH_y/H_2 blends. In the case in which the natural gas is injected with 10%, 25%, and 50% vol. H_2 , hydrogen embrittlement of base metal of tube body is less likely to occur. This conclusion was provided in respect to a threshold stress intensity factor criterion. The presented methodology is appropriate for evaluation of steels for pipelines carrying hydrogen-blended natural gas.

Acknowledgements

The authors wish to thank Corinth Pipeworks S.A. for facilitating the experimental data and Reviewers for their valuable comments and suggestions.

Received 3 August 2023

Appendix A.

Tensile, hardness tests and chemical composition of a 14.2 mm wall thickness L485ME steel grade [20].

Tensile and hardness tests results.

Base material (BM)				Spiral Weld (WM)			
No.	Heat No.	Yield Strength (MPa)	Tensile Strength (MPa)	Tensile Strength (MPa)	Hardness Max HV10		
					HAZ	Base	Weld
1.	0141335	503	626	635	207	213	227
2.	0141948	523	639	627	212	228	229
3.	0141261	491	614	660	222	222	233
4.	0141950	511	631	645	210	214	229
5.	0141149	529	643	638	215	222	231
6.	0141341	493	616	610	212	225	226
7.	0141427	490	613	659	209	221	228
8.	0141256	518	635	645	210	214	229
9.	0141950	511	631	662	210	220	227
10.	0141151	506	616	647	215	220	229

Chemical composition of L485ME steel grade [20].

No.	Heat No.	C %	Mn %	P %	S %	Si %	Cr %	Ni %	Mo %	Cu %	Ti %	Nb %	V %	Al %	Sn %	Ca %	N %	B %
1.	041335	0.065	1.583	0.0087	0.0028	0.293	0.022	0.036	0.002	0.013	0.0193	0.07	0.003	0.035	0.005	0.0017	0.0042	0.0001
2.	040948	0.065	1.600	0.0097	0.0035	0.280	0.04	0.036	0.003	0.015	0.0214	0.065	0.002	0.038	0.003	0.0021	0.0041	0.0001
3.	041261	0.067	1.565	0.0089	0.004	0.283	0.024	0.049	0.003	0.02	0.0217	0.069	0.002	0.041	0.003	0.0033	0.0044	0.0001
4.	041950	0.068	1.512	0.0113	0.0032	0.277	0.028	0.041	0.003	0.014	0.0223	0.054	0.003	0.0554	0.003	0.0026	0.0055	0.0001
5.	041149	0.065	1.569	0.0101	0.0032	0.285	0.034	0.041	0.008	0.014	0.0223	0.066	0.002	0.0431	0.005	0.0021	0.0042	0.0001
6.	041341	0.071	1.608	0.008	0.0038	0.286	0.017	0.038	0.002	0.015	0.0208	0.064	0.002	0.0398	0.003	0.0029	0.0045	0.0001
7.	041427	0.068	1.547	0.0097	0.0025	0.262	0.024	0.038	0.004	0.012	0.0217	0.058	0.001	0.0404	0.003	0.0028	0.0044	0.0001
8.	041256	0.065	1.531	0.0081	0.0028	0.278	0.022	0.038	0.002	0.014	0.0213	0.058	0.002	0.0384	0.003	0.0031	0.004	0.0001
9.	041950	0.068	1.512	0.0103	0.0033	0.277	0.028	0.041	0.003	0.014	0.0223	0.054	0.003	0.0554	0.003	0.0026	0.0055	0.0001
10.	041151	0.069	1.524	0.0095	0.0043	0.282	0.022	0.039	0.003	0.015	0.0212	0.059	0.002	0.0318	0.003	0.0035	0.0045	0.0001

Appendix B.

The experimental results of target and measured crack size, applied displacement target and applied stress intensity factor as well as stress intensity factor for 14.2 mm wall thickness tubes [20].

No.	Specimen ID	a_0 Target (mm)	V_m Applied (mm)	K_{IA} Target (MPa m ^{0.5})	a_0 Measured (mm)	K_{IA} Applied (MPa m ^{0.5})	$K_{IH,min}$ Minimum (MPa m ^{0.5})
1.	S203A-BM1	14.290	0.606	125.0	13.993	127.5	63.7
2.	S203A-BM2	14.690	0.621	125.0	14.956	123.1	61.5
3.	S203A-BM3	14.730	0.625	125.0	14.772	125.1	62.6
4.	S203A-BM4	14.570	0.619	125.0	14.206	128.3	64.1
5.	S203A-W1	14.060	0.599	125.0	14.667	120.7	60.3
6.	S203A-W2	14.700	0.625	125.0	14.632	126.2	63.1
7.	S203A-W3	14.470	0.614	125.0	13.473	133.2	66.6
8.	S203A-W4	14.200	0.606	125.0	14.882	120.5	60.3
9.	S203A-HAZ1	14.410	0.617	125.0	12.675	141.2	70.6
10.	S203A-HAZ2	14.530	0.619	125.0	15.132	121.4	60.7
11.	S203A-HAZ3	14.400	0.614	125.0	14.277	126.5	63.3
12.	S203A-HAZ4	14.630	0.619	125.0	13.874	130.8	65.4
13.	S203B-BM1	14.740	0.623	125.0	14.455	127.2	63.6
14.	S203B-BM2	14.990	0.635	125.0	11.720	156.1	78.1
15.	S203B-BM3	14.800	0.627	125.0	13.376	137.4	68.7
16.	S203B-BM4	14.450	0.617	125.0	13.242	135.9	68.0
17.	S203B-W1	14.260	0.606	125.0	13.657	129.8	64.9
18.	S203B-W2	14.530	0.616	125.0	14.125	128.1	64.1
19.	S203B-W3	14.320	0.611	125.0	13.850	129.3	64.6
20.	S203B-W4	14.460	0.647	125.0	14.725	129.8	64.9
21.	S203B-HAZ1	14.650	0.621	125.0	13.591	133.5	66.8
22.	S203B-HAZ2	14.550	0.619	125.0	14.389	126.7	63.4
23.	S203B-HAZ3	14.170	0.613	125.0	15.656	116.7	58.4
24.	S203B-HAZ4	14.510	0.618	125.0	14.287	127.3	63.6
25.	S203C-BM1	14.180	0.602	125.0	13.861	127.5	63.7
26.	S203C-BM2	15.180	0.639	125.0	13.755	136.4	68.2
27.	S203C-BM3	14.810	0.627	125.0	14.070	131.1	65.6

No.	Specimen ID	a_0	V_m	K_{IA}	a_0	K_{IA}	$K_{IH,min}$
		Target (mm)	Applied (mm)	Target (MPa m ^{0.5})	Measured (mm)	Applied (MPa m ^{0.5})	Minimum (MPa m ^{0.5})
28.	S203C-BM4	14.880	0.630	125.0	14.601	127.6	63.8
29.	S203C-W1	14.230	0.605	125.0	14.276	124.7	62.4
30.	S203C-W2	14.360	0.610	125.0	13.505	132.1	66.1
31.	S203C-W3	14.420	0.612	125.0	11.916	148.4	74.2
32.	S203C-W4	14.570	0.617	125.0	13.893	130.2	65.1
33.	S203C-HAZ1	14.670	0.628	125.0	12.711	143.2	71.6
34.	S203C-HAZ2	14.570	0.617	125.0	12.105	147.1	73.5
35.	S203C-HAZ3	14.490	0.616	125.0	14.028	128.8	64.4
36.	S203C-HAZ4	14.570	0.620	125.0	14.572	125.5	62.8

References

- [1] Cazenave P., Jimenez K., Gao M., Moneta A., Hryciuk P.: *Hydrogen assisted cracking driven by cathodic protection operated at near -1200 mV CSE - an onshore natural gas pipeline failure*. J. Pipeline Sci. Eng. **1**(2021), 1, 100–121.
- [2] Abdelghani M., Tewfik G., Witek M., Djahida D.: *Factors of Stress Concentration around Spherical Cavity Embedded in Cylinder Subjected to Internal Pressure*. Materials **14**(11) (2021).
- [3] Wasim M., Djukic M.B., Ngo T.D.: *Influence of hydrogen-enhanced plasticity and decohesion mechanisms of hydrogen embrittlement on the fracture resistance of steel*. Eng. Fail. Anal. **123**(2021), 105312.
- [4] Troiano A.R.: *The role of hydrogen and other interstitials in the mechanical behavior of metals*. Metallogr. Microstruct. Anal. **5**(2016), 6, 557–569.
- [5] Sofronis P., Birnbaum H.K.: *Hydrogen enhanced localized plasticity: A mechanism for hydrogen related fracture*. In: Fatigue and Fracture of Aerospace Structural Materials. American Society of Mechanical Engineers, Aerospace Division (Publication) AD, vol. 36, Publ. by ASME, pp. 15–25, Proc. 1993 ASME Winter Ann. Meet., New Orleans 1993.
- [6] Nguyen T.T., Park J., Kim W.S., Nahm S.H., Beak U.B.: *Effect of low partial hydrogen in a mixture with methane on the mechanical properties of X70 pipeline steel*, Int. J. Hydrogen Energy **45**(2020), 3, 2368–2381.
- [7] Nguyen T.T., Beak U.B., Park J., Nahm S.H., Tak N.: *Hydrogen environment assisted cracking in X70 welding heat-affected zone under a high-pressure hydrogen gas*. Theor. Appl. Fract. Mech. **109**(2020), 102746.
- [8] Alvaro A., Olden V., Macadre A., Akselsen O.M.: *Hydrogen embrittlement susceptibility of a weld simulated X70 heat affected zone under H2 pressure*. Mater. Sci. Eng. A **597**(2014), 29–36.

- [9] Golisch G., Genchev G., Wanzenberg E., Mentz J., Brauer H., Muthmann E., Ratke D.: *Application of line pipe and hot induction bends in hydrogen gas*. J. Pipeline Sci. Eng. **2**(2022), 3, 100067.
- [10] Ghosh G., Rostron P., Garg R., Panday A.: *Hydrogen induced cracking of pipeline and pressure vessel steels: A review*. Eng. Fract. Mech. **199**(2018), 609–618.
- [11] Krasovskii A.Y., Lokhman I.V., Orynyak I.V.: *Stress-corrosion failures of main pipelines*. Strength Mater. **44**(2012), 129–143.
- [12] Gangloff R.P., Somerday B.P.: *Gaseous Hydrogen Embrittlement of Materials in Energy Technologies*. In: *Mechanisms, Modelling and Future Developments*. Woodhead Publishing, 2012.
- [13] Wang R.: *Effects of hydrogen on the fracture toughness of a X70 pipeline steel*. Corros. Sci. **51**(2009), 12, 2803–2810.
- [14] Olden V., Alvaro A., Akselsen O.M.: *Hydrogen diffusion and hydrogen influenced critical stress intensity in an API X70 pipeline steel welded joint – experiments and FE simulations*. Int. J. Hydrogen Energy **37**(2012), 15, 11474–11486.
- [15] Zhou D., Li T., Huang D., Wu Y., Huang Z., Xiao W., Wang Q., Wang X.: *The experiment study to assess the impact of hydrogen blended natural gas on the tensile properties and damage mechanism of X80 pipeline steel*. Int. J. Hydrogen Energy **46**(2021), 10, 7402–7414.
- [16] EN-ISO 3183:2019. *Petroleum and natural gas industries - Steel pipe for pipeline transportation system*. Tech. rep. Tech. Comm., ISO/TC 67/SC 2 (2019).
- [17] API Spec 5L (46th Edn.), April 2018. *Line pipe*. Tech. rep., Washington.
- [18] ASME B31.12:2019. *Hydrogen piping and pipelines. ASME code for pressure piping*. Tech. rep., American Society of Mechanical Engineer, 2020.
- [19] ASME BPVC Section VIII, Division 3. *Alternative Rules for Construction of High Pressure Vessels. ASME Boiler and Pressure Vessel Code*, Tech. rep., American Society of Mechanical Engineer, 2021.
- [20] Corinth Pipeworks S.A.: *Hydrogen K_{IH} qualification test report K_{IH} testing of $40'' \times 14.2\text{mm}/L485\text{ME SAWH}$. 2022 (non-published)*.
- [21] ASTM E1681-03. *Standard Test Method for Determining Threshold Stress Intensity Factor for Environment Assisted Cracking of Metallic Materials*. ASTM Int. Tech. rep., 2020.
- [22] Uilhoorn F.E.: *Comparison of Bayesian estimation methods for modeling flow transients in gas pipelines*. J. Nat. Gas Sci. Eng. **38**(2017), 159–170.
- [23] Witek M., Uilhoorn F.: *Impact of hydrogen blended natural gas on linepack energy for existing high pressure pipelines*. Arch. Thermodyn. **43**(2022), 3, 111–124.
- [24] Techo R., Tickner R.R., James R.E.: *An accurate equation for the computation of the friction factor for smooth pipes from the Reynolds number*. J. Appl. Mech. **32**(1965), 2, 443–443.
- [25] Kreith F., Bohn M.S.: *Principles of Heat Transfer* (5th Edn.). West Publ., St Paul 1993.

- [26] Kunz O., Wagner W.: *The GERG-2008 Wide-Range equation of state for natural gases and other mixtures: An expansion of GERG-2004*. J. Chem. Eng. Data **57**(2012), 11, 3032–3091.
- [27] Schiesser W.E.: *The Numerical Method of Lines: Integration of Partial Differential Equations*. Academic Press, San Diego 1991.
- [28] Bank R.E., Coughran W.M., Fichtner W., Grosse E.H., Rose D.J., Smith R.K.: *Transient simulation of silicon devices and circuits*. IEEE Trans. Electron Devices **32**(1985), 10 1992–2007.
- [29] Hosea M.E., Shampine L.F.: *Analysis and implementation of TR-BDF2*. Appl. Numer. Math. **20**(1996), 1, 21–37.
- [30] Shampine L.F., Reichelt M.W.: *The MATLAB ODE suite*, SIAM J. Sci. Comput. **18**(1997), 1, 1–22.
- [31] Fukai Y.: *The Metal-Hydrogen System: Basic Bulk Properties*. Springer Science & Business Media, 2006.
- [32] Kirchheim R., Pundt A.: *25 – Hydrogen in Metals*. In: Physical Metallurgy (5th Edn.) (D.E. Laughlin, K. Hono, Eds.), Elsevier, Oxford 2014, 2597–2705.
- [33] Drexler A., Konert F., Sobol O., Rhode M., Domitner J., Sommitsch C., Böllinghaus T.: *Enhanced gaseous hydrogen solubility in ferritic and martensitic steels at low temperatures*. Int. J. Hydrogen Energy **47**(2022), 93, 39639–39653.
- [34] Kirchheim R.: *Solubility, diffusivity and trapping of hydrogen in dilute alloys. deformed and amorphous metals – II*. Acta Metall. **30**(1982), 6, 1069–1078.
- [35] ASTM E399-22. *Standard Test Method for Linear-Elastic Plane-Strain Fracture Toughness K_{IC} of Metallic Materials*. ASTM Int. Tech. rep., 2022.
- [36] Skjellerudsveen M., Akselsen O., Olden V., Johnsen R., Smirnova A.: *Effect of microstructure and temperature on hydrogen diffusion and trapping in X70 grade pipeline steel and its weldments*. In: Proc. Eur. Corrosion Conf., Moscow, 13-17 Sept. 2010.
- [37] Uilhoorn F.E.: *Dynamic behaviour of non-isothermal compressible natural gases mixed with hydrogen in pipelines*. Int. J. Hydrogen Energy **34**(2009), 16, 6722– 6729.
- [38] Drexler A., Depover T., Leitner S., Verbeken K., Ecker W.: *Microstructural based hydrogen diffusion and trapping models applied to Fe-CX alloys*. J. Alloys Compd. **826**(2020), 154057.